Model-based Catalyst Selection for the Oxidative Coupling of Methane in an Adiabatic Fixed-Bed Reactor

Laura Pirro[†], Ana Obradović[†], Bart D. Vandegehuchte[‡], Guy B. Marin[†], Joris W. Thybaut[,†]*

† Laboratory for Chemical Technology, Ghent University, Technologiepark 914, B-9052 Ghent, Belgium

‡ Total Research & Technology Feluy, Zone Industrielle Feluy C B-7181, Seneffe, Belgium

ABSTRACT: Adiabatic operation of catalytic fixed-bed reactors for Oxidative Coupling of Methane (OCM) has been simulated using a detailed microkinetic and reactor model. For several catalysts ($1\%_{wt}Sr/La_2O_3$, $10\%_{wt}La\text{-}20\%_{wt}Sr/CaO$, $4\%_{wt}Sn\text{-}2\%_{wt}Li/MgO$ and $12\%_{wt}Mn\text{-}20\%_{wt}Na_2WO_4/SiO_2$), diverse in activity and selectivity towards C_{2+} products, operating conditions have been determined that maximize C_{2+} yield at low inlet temperature T_0 (<< 923 K). A prior analysis of light-off curves served as a guideline for optimal operating temperature ranges for each catalyst.

Imposing a maximum temperature in the reactor ($T^{max} \leq$ 1273 K) suggested a limit for the catalytic performances, corresponding to 13% CH_4 conversion and 61% C_{2+} selectivity at the reactor outlet for an active (T_0= 723 K) Sr/La_2O_3 catalyst, and an improved 19% CH_4 conversion and 82% C_{2+} selectivity for a less active (T_0= 853 K) $NaMnW/SiO_2$ catalyst. The obtained

results indicated catalyst selectivity, rather than activity, as the key parameter for an industrially relevant adiabatic OCM process.

1. INTRODUCTION

Oxidative Coupling of Methane (OCM) has been under the academic spotlight for the last 36 years[1] thanks to its potential to convert methane-rich feedstocks directly into added-value chemicals[2], rather than via synthesis gas. Methane is the main constituent of many abundant resources such as natural gas[3], shale gas[4] and biogas[5]. Ethylene, the desired product of OCM, is situated at the heart of the petrochemical industry[6] and its production is globally achieved via steam cracking, which, unfortunately, is not economically viable for small scale applications or for stranded gas reservoirs[7].

The economic driver has raised ubiquitous interest toward the OCM process in the last decades. The drawbacks that have so far hampered its industrial implementation can be understood by from the chemistry and the thermodynamics of the key global reactions:

$CH_4 + 0.25\ O_2 \rightarrow 0.5\ C_2H_6 + 0.5\ H_2O$ $\quad \Delta_r H^0 = -88\ \text{kJ/mol}_{CH4}$

$CH_4 + 0.5\ O_2 \rightarrow 0.5\ C_2H_4 + H_2O$ $\quad \Delta_r H^0 = -141\ \text{kJ/mol}_{CH4}$

$C_2H_6 + 3.5\ O_2 \rightarrow 2CO_2 + 3H_2O$ $\quad \Delta_r H^0\ -1429\ \text{kJ/mol}_{C2H6}$

$C_2H_4 + 3O_2 \rightarrow 2CO_2 + 2H_2O$ $\quad \Delta_r H^0 = -1324\ \text{kJ/mol}_{C2H4}$

The hydrocarbon products (C_2H_6 and C_2H_4), as well as the primary reactant (CH_4) itself, can undergo total oxidation. As C_2 hydrocarbons are more reactive than methane[8], the maximum achievable C_{2+} yield at relevant operating conditions is limited by the inverse relationship between CH_4 conversion and C_{2+} selectivity[9].

Furthermore, coupling to C_{2+} products is exothermic, but the exothermicity of competitive oxidation is much more pronounced. Considering that the threshold for catalytic methane

activation in OCM is situated typically around 923 K[10], such thermal power release at high temperatures causes safety and operational concerns that jeopardize the scale-up of the reaction[11].

These challenges have been tackled through optimization studies about catalytic materials[12], reactor configurations[13] and process layouts[14, 15], with a specific focus on C_{2+} selectivity and yield maximization. Concerning OCM exothermicity, a wave of new studies has arisen from the idea of exploiting the thermal power generated by the reaction, instead of just considering it as a nuisance to be handled. The ignition and extinction of the reaction has in fact been investigated for powder[16, 17], pellet[18] and nanofiber catalysts[19, 20] and this has led to the concept of 'autothermal' OCM reactors[21, 22]. In the present context 'autothermal' indicates that the process can be self-sustained thanks to the thermal power generated by the reaction; the operation of the reactor is therefore shifted towards lower inlet temperatures, which results in reduced CAPital and OPerational Expenses.

Low inlet temperature operation is one of the features of the Siluria OCM process, which, following the opening of a demonstration facility in 2015 in La Porte (Texas, USA), is so far the only company that claims to come close to the commercialization of OCM[23]. The low inlet temperature solution proposed by Siluria includes an adiabatic fixed-bed reactor for OCM[24]. The gas mixture is heated up along the reactor thanks to the OCM exothermicity and the higher temperatures achieved at the outlet are exploited to perform ethane dehydrogenation of a secondary stream in a post-bed cracking section[25].

While the majority of the laboratory scale reactors is operated in a pseudo-isothermal regime[26, 27], adiabatic operation seems the only technical solution to fixed-bed industrial-scale reactors[17], thus urging on re-evaluating and comparing the performance of OCM catalysts in adiabatic mode. OCM is in fact characterized by a peculiar two-way relationship between temperature and selectivity: on one hand the adiabatic temperature rise is influenced by the selectivity[28],

with non-selective oxidation reactions being more exothermic than the C-C coupling; on the other hand the maximum achievable C_{2+} selectivity increases with temperature[29], thanks to the formation rate of surface methyl radicals surpassing the rate of methane oxidation. For each catalyst, fine-tuning of the operating conditions is therefore vital to reach an optimal trade-off between a low inlet temperature and a high C_{2+} selectivity and yield. In addition, operational constraints need to be taken into account with respect to safety such as respecting the maximum temperature allowed by the metallurgy of the reactor.

The present simulation study aims at elucidating the yield-temperature relationship in adiabatic fixed-bed reactors for OCM and to provide guidelines for catalyst selection in the industrially-relevant OCM process in adiabatic mode. Considering that the operating temperature range is an important performance criterion, both in terms of inlet and maximum reactor temperature, analyzing simulated light-off curves[30] aids considerably in comparing the performance of OCM catalysts. In the present context, light-off curves report the oxygen conversion at the outlet of the OCM reactor as a function of the gas inlet temperature.

Adiabatic OCM has already been studied in the past using simulation models based on global kinetic schemes[31-33], such as the one from Stansch et al.[34]. However, these models are usually less reliable outside their design range, which definitely did not include adiabatic test data. In the present study, adiabatic OCM is investigated by using a detailed descriptor-based microkinetic model[35], which does not assume any rate-determining step and guarantees thermodynamic consistency through catalytic cycles, therefore resulting in high flexibility in describing the reaction chemistry with varying operating conditions and different catalysts.

In the first part of the work, the essential features of the previously developed microkinetic model are summarized[35-37], together with the adiabatic reactor model equations. The fixed-bed reactor is modelled as a 1D heterogeneous Plug Flow Reactor (PFR), therefore none of the ignition/extinction phenomena arising from multiplicity of steady states are aimed at. For the

readers specifically interested in such phenomena, very recent, more dedicated literature on the topic is available[27, 38, 39]. Instead, the present work specifically focuses on the so-called 'light-off' behavior. Background information on light-off curves is provided, clarifying the adopted terminology and exploring their applicability to adiabatic OCM. Subsequently, the adiabatic simulation results are presented and discussed in three sections: the first one zooming in on the key features of adiabatic operation, the second section on light-off curves obtained for four OCM catalysts, and the final section evaluating the impact of operational constraints on the overall performance and on the criteria for catalyst selection.

It should be mentioned that the present simulations do not take catalyst deactivation with time-on-stream into account. Nevertheless, qualitative trends in the catalytic performances can be established specifically for start-of-run activities in adiabatic OCM.

2. MODELLING TOOLS

2.1 Microkinetic Model

The OCM reaction kinetics were calculated according to a detailed microkinetic model, which accounts for the complex chemistry of the reactions occurring both in the gas phase and on the catalyst surface. The microkinetic model comprises 39 reversible gas-phase reactions and 26 reversible reactions on the catalyst surface[35]; see Tables S1 and S2 in the Supporting Information for more details. The species which have been considered are: 13 molecules (H_2, H_2O, H_2O_2, O_2, CH_4, CH_2O, CO, CO_2, C_2H_2, C_2H_4, C_2H_6, C_3H_6, C_3H_8), 10 radicals ($H\cdot$, $O\cdot$, $OH\cdot$, $HO_2\cdot$, $CHO\cdot$, $CH_3O\cdot$, $CH_3\cdot$, $C_2H_3\cdot$, $C_2H_5\cdot$, $C_3H_7\cdot$) and 10 surface species ($O*$, $OH*$, H_2O*, $CO*$, CO_2*, $CHO*$, CH_2O*, CH_3O*, C_2H_3O*, C_2H_4O*), plus the free active sites $*$**.** The gas-phase reaction network is based on free-radical mechanisms widely adopted in combustion chemistry, with the kinetic parameters regressed towards non-catalytic OCM experimental data; furthermore, the mechanism has been reduced via sensitivity and contribution analyses. The

surface reaction network is based on catalytic cycles and thermodynamic consistency within these cycles; it describes the overall reaction in terms of elementary steps involving adsorbed reactants, products, and reaction intermediates associated with active sites, without assuming any rate-determining step. The implementation of thermodynamic relationships in a microkinetic model is one approach in relating kinetic parameters to catalyst properties and simultaneously reducing the number of adjustable parameters. The model parameters are classified into kinetic and catalyst descriptors. The former do not depend on the catalyst, but relate purely to the reaction kinetics, whereas the catalyst descriptors represent the physical and chemical properties that are characteristic of the specific features of the different catalysts that have been investigated[37]. The use of catalyst descriptors, such as the chemisorption enthalpy, the sticking probability and the active site density, allows formulating properties-performance relations via the reaction kinetics. These descriptors are typically obtained via model regression using isothermal experimental data and the performance of different catalytic materials can be simulated without any prior assumptions on the rate-determining step and the dominant pathway. A detailed explanation of the descriptors used in the OCM kinetic model has been provided in the previous works[36], and herein a summary is reported in Table S3 of the Supporting Information.

The microkinetic model has proven to be successful in describing experimental data over 5 different catalysts in a broad range of operating conditions; with some modifications in the kinetic parameters, it has also been used by other research groups to reproduce experimental data obtained for nanofiber fabric catalysts[40]. In the present work, the following catalysts are considered: $10\%_{wt}La\text{-}20\%_{wt}Sr/CaO$[37], $1\%_{wt}Sr/La_2O_3$[36], $4\%_{wt}Sn\text{-}2\%_{wt}Li/MgO$[35] and $12\%_{wt}Mn\text{-}20\%_{wt}Na_2WO_4/SiO_2$[26]. The physical and chemical properties used for the modelling purposes can be found in the above referred literature.

2.2 Reactor Model

OCM kinetics were implemented into an adiabatic Plug Flow Reactor (PFR) model, which accounts for irreducible transport limitations of radicals[35] . The reactor model is:

- 1-Dimensional: no radial concentration and temperature gradients are considered on the reactor scale; only the dimensionless axial coordinate $z \in [0,1]$ is accounted for on the reactor scale; $z = x/L$, where $x \in [0,L]$ is the axial coordinate and L is the reactor length.
- Heterogeneous: on the particle-scale two different phases are considered. The *intraparticle* phase consists of the catalyst particles and the gas contained in their pores; the *interstitial* phase accounts for the gas around the particles. These two phases are represented by two different coordinate systems on the particle scale. The *intraparticle* phase is described using spherical symmetry by the radial coordinate $\xi \in [0, d_P/2]$, where 0 is the center of the catalyst particle and $d_P/2 = r_P$ is the particle radius. The *interstitial* phase is described using cylindrical symmetry by the radial coordinate $r \in [0, d_V/2]$, where 0 is the center of the gas phase and d_V is the characteristic dimension of the *interstitial* phase, i.e. the average distance between two catalyst particles.

The thermal power generated by the reaction was included in an adiabatic energy balance, where axial solid conduction on the reactor scale was considered negligible. This assumption is part of the ideal PFR model, without axial dispersion, and therefore applies to reactors with high (> 50) L/d_p ratio[41], operated at high (> 10) Peclet numbers, and in an operating range leading to low (< 40) Zeldovich numbers, namely high (>> 300K) inlet temperatures and high (> 8) methane-to-oxygen inlet ratios[38].

The balance equations and the corresponding boundary conditions are reported in Table 1. For a detailed description and the corresponding list of symbols, the reader is referred to paragraph 4 of the Supporting Information.

Table 1. Adiabatic Reactor Model Equations.

	Interstitial Phase	Intraparticle Phase
Mass Balance[35]	$\frac{F_V}{A_s}\frac{\partial C_{i,g}}{\partial z} - \varepsilon_b \frac{D_{m,i}}{r}\frac{\partial}{\partial r}\left(r\frac{\partial C_{i,g}}{\partial r}\right) = \varepsilon_b R_{i,g}$	$-\frac{D_{e,i}}{\xi^2}\frac{\partial}{\partial \xi}\left(\xi^2\frac{\partial C_{i,c}}{\partial \xi}\right) = \varepsilon_c\, R_{i,g} + R_{i,c}$
Boundary Conditions[35]	$z = 0 \ \wedge 0 < r < \frac{d_V}{2}, C_{i,g} = C_{i,0}$	$\xi = 0, \frac{\partial C_{i,c}}{\partial \xi} = 0$
	$z > 0 \ \wedge r = 0, \frac{\partial C_{i,g}}{\partial r} = 0$	
	$z > 0 \ \wedge r = \frac{d_V}{2}$, $-a_g D_{m,i}\frac{\partial C_{i,g}}{\partial r} = a_c D_{e,i}\frac{\partial C_{i,c}}{\partial \xi}$	$\xi = \frac{d_P}{2}, C_{i,g} = C_{i,c}$
Energy Balance	$\frac{F_W\, C_{p,g}}{A_s}\frac{\partial T_g}{\partial z} = \frac{\lambda_g}{r}\frac{\partial}{\partial r}\left(r\frac{\partial T_g}{\partial r}\right) - \varepsilon_b\, \dot{Q}_g^{interst}$	$\forall \xi: T_c = const.$
Boundary Conditions	$T_g = T_0$	$\xi = \frac{d_p}{2}: T_c = T_g$
	$z = 0, \forall r: \frac{\partial T_g}{\partial r} = 0$	
	$z > 0 \ \wedge r = \frac{d_v}{2}$, $a_g \lambda_g \frac{\partial T_g}{\partial r} = (1-\varepsilon_b)\left[\varepsilon_c\, \overline{\dot{Q}_g^{intrap}} + \overline{\dot{Q}_c^{intrap}}\right]$	

A schematic representation of the reactor model considered in the present work is reported in Figure 1. It can be observed that two different temperatures are considered on the particle scale: the temperature of the *interstitial* phase (only gas), T_g, and the temperature of the *intraparticle* phase (solid + gas), T_c. The difference between the two phases is accounted for due to the low thermal conductivity of the gas that results in temperature gradients in the *interstitial* phase; on the other hand, the solid conductivity of a single catalyst particle is sufficiently high to assume particle isothermicity. More detailed information about the relative importance of *intraparticle* and *interstitial* temperature gradients are reported in paragraph 5 of the Supporting Information.

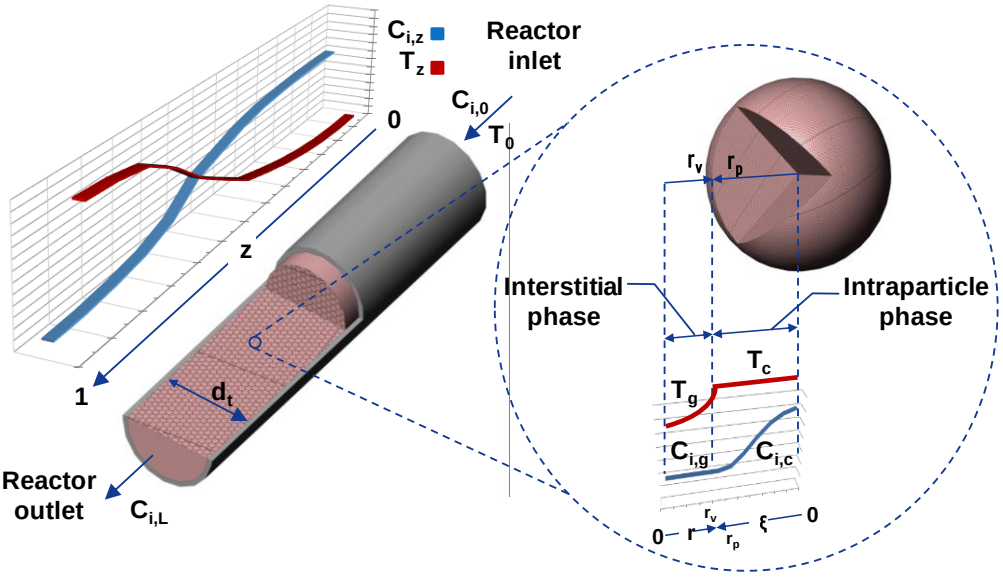

Figure 1. Schematic representation of the heterogeneous 1-D fixed-bed reactor model; adapted from [35].

In order to simplify the interpretation of the results, when a temperature profile is shown in the following paragraphs, only one temperature is reported at each coordinate along the reactor, i.e. the average value of the temperature of the *interstitial* and the *intraparticle* phase. This graphical simplification does not affect the validity of our conclusions, because, given the oxygen-lean operating conditions and the small particle dimension (≤ 300 μm) of the simulated catalysts, the difference between the temperature at the center of the *interstitial* phase and the particle surface in the present study is negligible (rate deviations < 2%[42]). Care should be taken when extrapolating the results of the present work to cases where these local gradients would not be negligible, because in case of such an exothermic reaction as OCM they might represent a source of multiplicity of steady states[43].

2.3 Light-off Curves

Given a specific catalyst and a fixed set of operating conditions, a light-off curve shows the conversion of the limiting reagent at the outlet of a catalyst bed as a function of the fluid inlet temperature T_0[30]. Light-off curves traditionally pertain to the domain of exhaust treatment research[44], but adiabatic OCM operation clearly shows an analogy with the cold-start of a

catalytic converter: an active catalyst initiates the reaction desirably at the lowest temperature possible to, in the case of OCM, minimize the external energy input required.

In addition to well-known applications in the design and optimization of Diesel Oxidation Catalysts (DOC)[45] and Three Way Catalytic Converters (TWC)[46], light-off curves have been employed to analyze other catalytic oxidation reactions, such as toluene[47], formaldehyde[48], ammonia[49] and, more extensively, methane[50] combustion. For all reactions mentioned above, light-off curves referred to the conversion of a pollutant/fuel as the limiting reagent that was completely oxidized at the outlet of the reactor. However, if the focus is shifted from fuel conversion to oxidant conversion, light-off curves can be useful for other exothermic, catalytic reactions where the oxidant is fed in sub-stoichiometric amounts to prevent full oxidation of a carbon-based feed. Some notable examples are syngas production via Catalytic Partial Oxidation (CPOX)[51] and the Oxidative Dehydrogenation (ODH) of ethane[52]. OCM belongs to this group of 'oxygen-limited' reactions, the reacting mixture always being rich in methane (reactant inlet molar ratio $CH_4/O_2|_{z=0} > 2$)[53].

Therefore, in the present work, light-off curves for OCM catalysts report the oxygen conversion X_{O2} at the outlet reactor as a function of the gas inlet temperature T_0.

The inlet temperature leading to 50% conversion of the limiting reagent ($T_0|X_{O2}= 50\%$) is defined as the light-off temperature (T_{LO})[54] and it is usually close to the inflection point in the light-off curve. Vandewalle et al.[39] have demonstrated that the unicity of the steady-state for OCM is satisfied when the reaction takes place in a PFR, therefore, only one light-off temperature can be identified for each combination of catalyst and operating conditions.

Another variable of interest in the present study is the minimum inlet temperature required for complete oxygen conversion ($T_0^{min}|X_{O2}= 100\%$), as it represents the industrially most feasible operating point, and is here indicated with T_0*.

A third relevant parameter is the slope of the curve in the proximity of T_{LO}; this is indicated with tgα and is calculated as: $tg\alpha = \frac{dX_{O_2}}{dT_0}|_{T_0=T_{LO}}$

3. SIMULATION RESULTS AND DISCUSSION

3.1 Adiabatic vs isothermal operation: a case study

In this section, a case study on a selected benchmark catalyst is briefly presented to highlight the key characteristics of an OCM adiabatic reactor in terms of temperature and concentration profiles. The $1\%_{wt}Sr/La_2O_3$ catalyst seems particularly promising for adiabatic operation thanks to its high thermal resistance[55], and has therefore been chosen for the present case study.

A typical simulation result of adiabatic OCM is reported in Figure 2 (red bars) in terms of CH_4 conversion, and C_{2+} selectivity and yield. The operating conditions are the following: inlet temperature T_0= 840 K, total pressure p_t= 150 kPa, reactants molar inlet ratio $CH_4/O_2|_{z=0}$= 12, gas hourly space velocity GHSV= 35000 h^{-1}, space time $W/F_{CH4,0}$= 3.45 kg_{cat} s/$mol_{CH4,0}$, no gas-phase dilution.

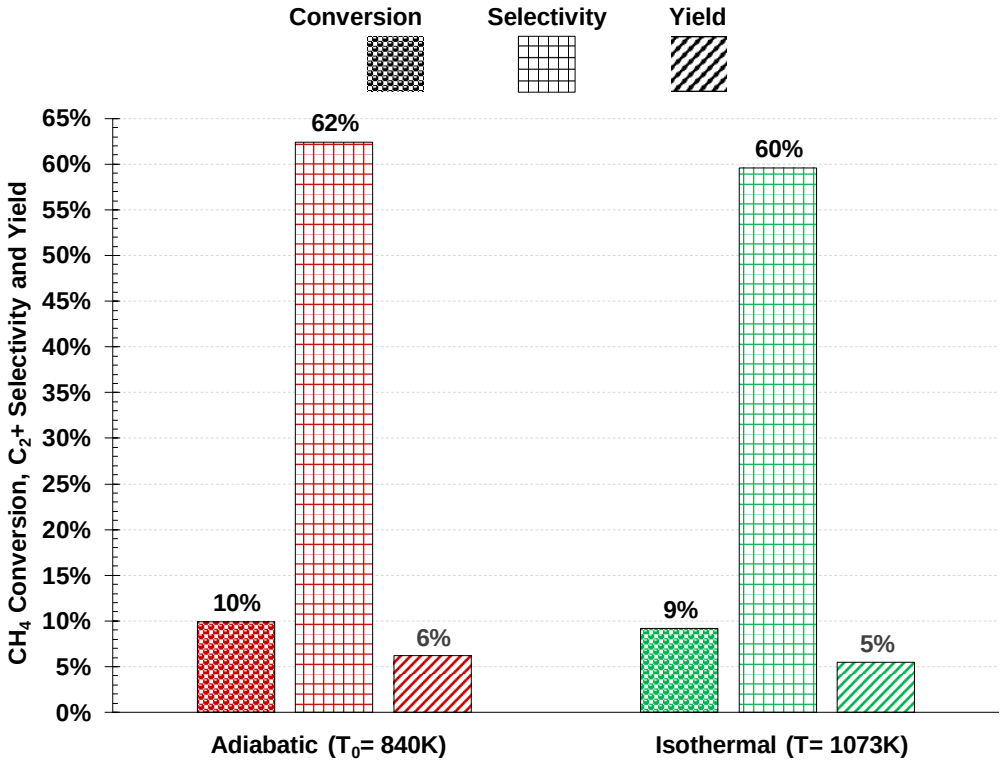

Figure 2. Adiabatic and isothermal simulated performances of a 1%$_{wt}$Sr/La$_2$O$_3$ fixed-bed reactor. The operating conditions are the following: Adiabatic – T_0= 840 K, GHSV≅ 35000 h^{-1}, W/F$_{CH4,0}$= 3.45 kg$_{cat}$ s/mol$_{CH4,0}$; Isothermal – T= 1073 K, W/F$_{CH4,0}$= 0.34 kg$_{cat}$ s/mol$_{CH4,0}$, GHSV≅ 350000 h^{-1}. For both cases: p_r= 150 kPa, CH$_4$/O$_2$|$_{z=0}$= 12, complete oxygen conversion in correspondence to the reactor outlet.

The inlet temperature value has been set to an arbitrary value lower than the minimum temperature used for isothermal tests (i.e. < 923 K). A low pressure has been chosen in line with the majority of literature data and following the negative impact of high pressure on OCM gas-phase kinetics[56]. The pronounced excess of methane (reactants inlet ratio 6-fold higher than stoichiometrically required for ethylene production) is in accordance with previous literature[32] and should lead to a gradual and limited temperature increase along the catalyst bed. The space time has been adapted so as to exactly establish complete oxygen conversion at the reactor outlet. Further investigation of methane and C_2 gas-phase reactivity after the point of oxygen depletion is beyond the scope of the present work, given the focus on the comparison of catalytic performances.

Throughout this work, only the combinations of operating conditions leading to complete oxygen conversion are considered in view of commercial interest. Additionally, this approach

alleviates the safety concerns, which would arise in a facility downstream the OCM reactor in presence of residual oxygen. The C_{2+} yield at complete oxygen conversion is further denoted as the C_{2+} *ultimate* yield, being the maximum value that can be achieved by a catalyst at a given set of operating conditions. The *ultimate* yield is therefore a critical parameter in catalyst selection.

As a reference for this case study, the same catalytic bed was simulated in the case of perfect isothermicity at T = 1073 K. This reaction temperature has been chosen in order to achieve performances comparable to the adiabatic case in terms of conversion and selectivity at the reactor outlet. The results corresponding to simulated isothermal operation are reported in green in Figure 2. These results are obtained assuming an ideally perfect cooling strategy, which enables to obtain the same temperature in each point of the reactor and results in no hotspot. It is therefore clear that this assumption is not representative of the actual situation in the majority of the pseudo-isothermal experimental set-ups[11] and in the present work, as suggested also in previous literature[31], it represents a model benchmark, as opposed to the model case of a perfectly adiabatic reactor.

Figure 2 highlights the key distinguishing feature of adiabatic operation of the fixed-bed reactor: catalytic performances (X_{CH4}= 10%, S_{C2+}= 62%, Y_{C2+}= 6%) comparable to the ones in a perfectly isothermal operation (X_{CH4}= 9%, S_{C2+}= 60%, Y_{C2+}= 5%) were obtained, for this specific case study, by feeding a more than 200 K 'colder' gas stream.

To ensure complete oxygen conversion, the space time was varied in both cases: for the isothermal reactor a 10 times lower space time ($W/F_{CH4,0}$= 0.34 kg_{cat} s/$mol_{CH4,0}$) was sufficient to achieve complete oxygen depletion at the reactor outlet compared to the adiabatic case. The higher space time used in the adiabatic case was in fact necessary to compensate for the low activity at low temperature and this represents another major difference between the two operating modes.

Despite the comparable performances obtained at the outlet, the reaction development along the reactor in the two model cases was completely different, as can be observed from the oxygen molar fraction axial profiles shown in Figure 3.A. In the adiabatic case, the oxygen conversion mainly occurred in the final part of the reactor, with approximately 90% of the catalyst bed barely exhibiting activity, due to the low temperature. In Figure 3.B it can be observed that, due to the thermal power generated by the reaction, an adiabatic temperature rise amounting to 394 K was simulated, leading to an outlet temperature of 1234 K. This temperature increase caused the boost in the conversion observed in Figure 3.A.

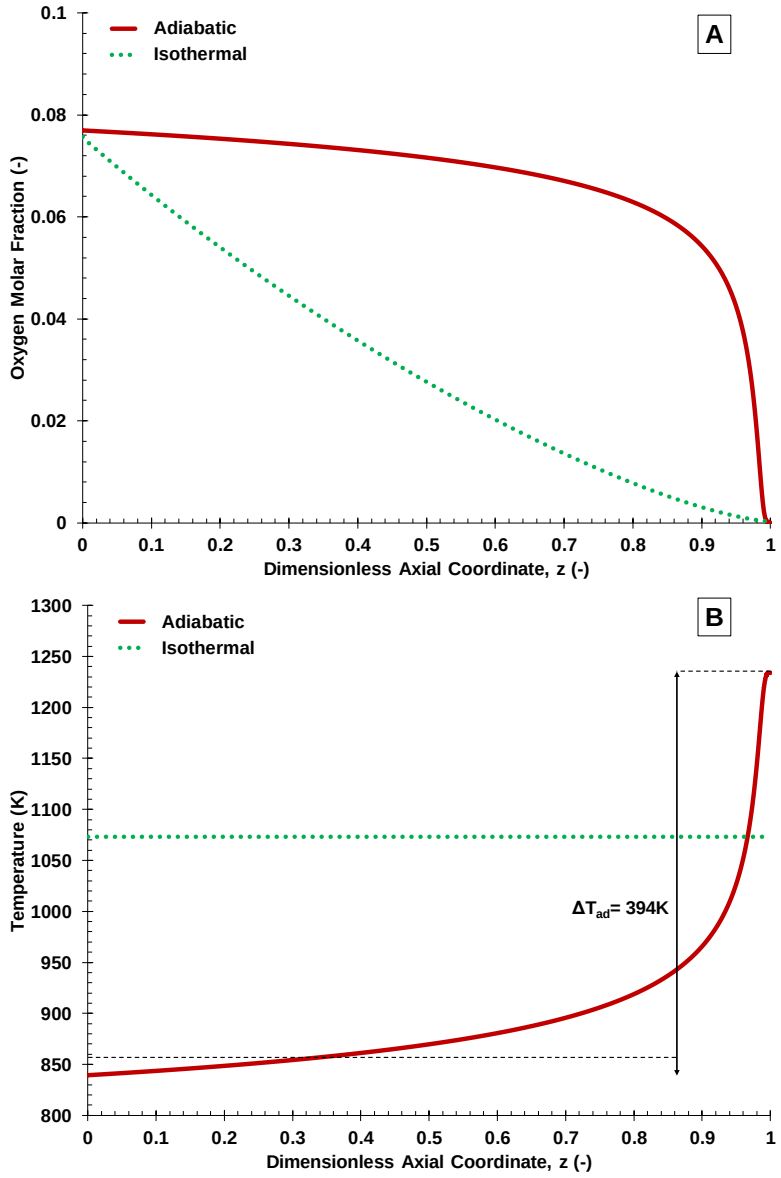

Figure 3. Oxygen molar fraction and temperature axial profiles for the two cases reported in Figure 2.

A similar trend can be observed in Figure 4, where the particle-reactor scale concentration field of $CH_3\cdot$ is reported for both the adiabatic (A) and the isothermal (B) case.

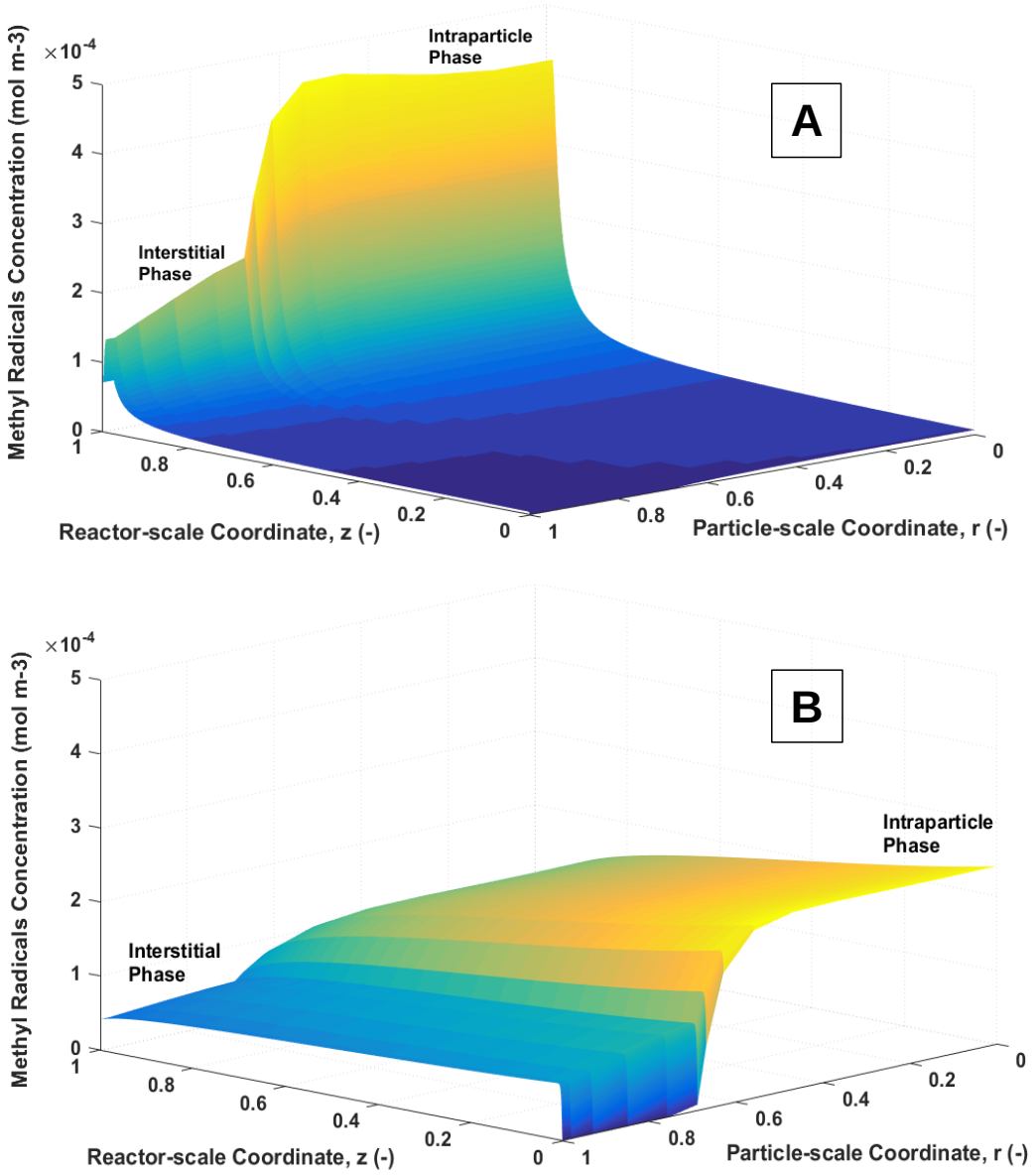

Figure 4. Particle-reactor scale 3-D fields of $CH_3\cdot$ concentration in case of adiabatic (A) and isothermal (B) operation for the case study described in Figures 2 and 3. On the particle-scale coordinate, 0 corresponds to the center of the catalyst particle.

For highly reactive species such as radicals, particle-scale transport phenomena play a crucial role in the overall catalytic bed performances. We therefore zoom in on the concentration profiles from both the reactor and the particle scale. As already reported in previous literature about isothermal OCM[35], the $CH_3\cdot$ radical concentration is higher in the *intraparticle* phase

than in the *interstitial* phase, since $CH_3\cdot$ is mainly formed via methane activation on the catalyst surface. The concentration decreases significantly in the proximity of the particle external surface, due to the diffusion barrier towards the *interstitial* phase. In the adiabatic case (Figure 4.A), the $CH_3\cdot$ concentration profile along the reactor coordinate follows the same trend as the temperature: a sharp temperature increase at approximately 90% of the reactor length provokes a boost in the reaction rates and, hence, in the $CH_3\cdot$ radical concentration, of which the maximum value is roughly double compared to the one from the isothermal case. The adiabatic $CH_3\cdot$ profile is non-monotonous: the concentration peak corresponds to the temperature peak in Figure 3.B, which is linked to complete oxygen depletion, as shown in Figure 3.A. Finally, it is worth highlighting that the concentration differences between the *intraparticle* and *interstitial* phase, which are present also in isothermal operation (Figure 4.B), are magnified in the terminal part of the adiabatic reactor where mass transport limitations for the radicals are more pronounced due to the high temperature.

3.2 Comparison of OCM catalysts by means of light-off curves

Exploiting the thermal power generated by the reaction and the consequent adiabatic temperature rise along the reactor axis, it was demonstrated that OCM catalysts should not be evaluated simply in terms of C_{2+} yield, but also in terms of the minimum inlet temperature achieving those yields. Light-off curves were employed herein as preliminary screening tools to compare the operating temperature ranges for different OCM catalysts.

Figure 5 reports the light-off curves for the four investigated catalysts ($10\%_{wt}La\text{-}20\%_{wt}Sr/CaO$, $1\%_{wt}Sr/La_2O_3$, $4\%_{wt}Sn\text{-}2\%_{wt}Li/MgO$ and $12\%_{wt}Mn\text{-}20\%_{wt}Na_2WO_4/SiO_2$), simulated at the same operating conditions as reported in Figure 2: total pressure p_t= 150 kPa, reactants molar inlet ratio $CH_4/O_2|_{z=0}$= 12, gas hourly space velocity GHSV= 35000 h^{-1}, space time $W/F_{CH4,0}$= 3.45 $kgcat\ s/mol_{CH4,0}$, no gas-phase dilution. The investigated temperature ranges were adapted

for each catalyst in order to be able to obtain the full curve, up to complete oxygen conversion. The corresponding values for T_{LO} and T_0* are indicated on the graph.

Each data point of the reported curves represents a potential operating point for that particular catalyst and contains a substantial amount of information, such as concentration fields, adiabatic temperature rise and performance at the outlet of the reactor. As an example, it can be highlighted that the adiabatic case study previously shown in Figures 2, 3 and 4 corresponds to the point (840 K,100%) on the orange curve, pertaining to the $1\%_{wt}Sr/La_2O_3$ catalyst.

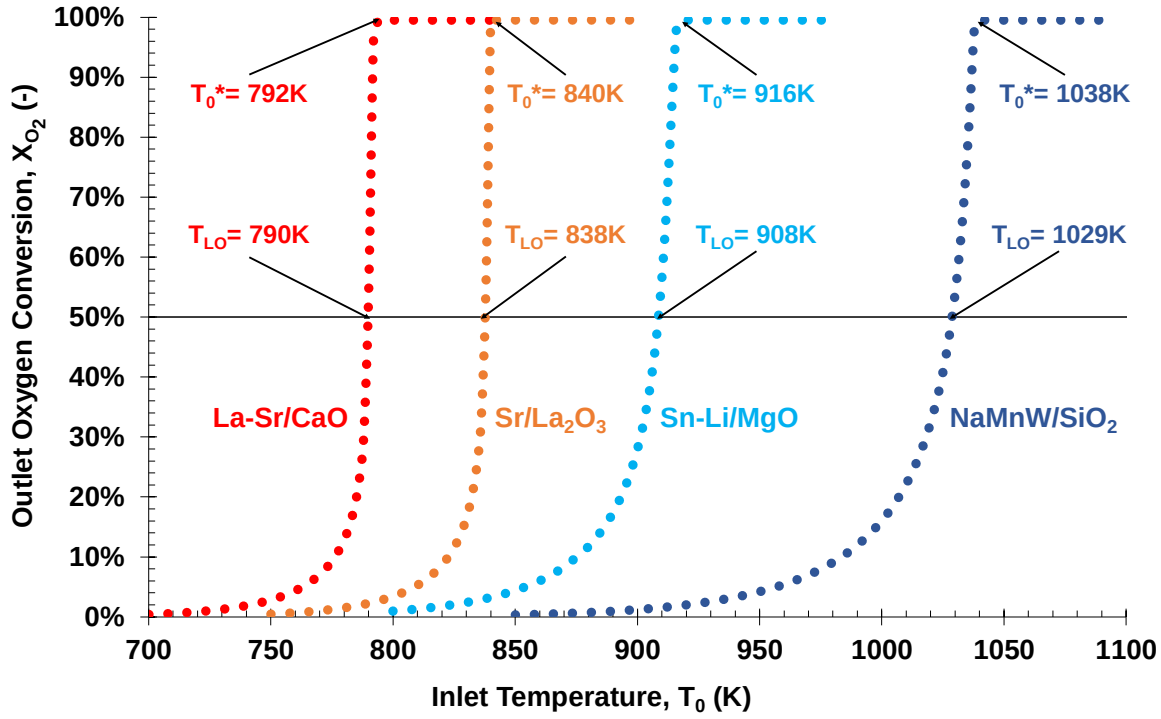

Figure 5. Light-off curves for 10%wtLa-20%wtSr/CaO, $1\%_{wt}Sr/La_2O_3$, $4\%_{wt}Sn$-$2\%_{wt}Li/MgO$ and $12\%_{wt}Mn$-$20\%_{wt}Na_2WO_4/SiO_2$. Operating conditions: p_t= 150 kPa, $CH_4/O_2|_{z=0}$= 12, GHSV= 35000 h^{-1}, $W/F_{CH4,0}$= 3.45 kg_{cat} $s/mol_{CH4,0}$, no gas-phase dilution.

The order of increasing catalyst activity ($NaMnW/SiO_2$ < Sn-Li/MgO < Sr/La_2O_3 < La-Sr/CaO), which follows the order of decreasing light-off temperatures (1029 K > 908 K > 838 K > 790 K), corresponds well with the activity order observed at isothermal conditions as reported in the literature for the investigated catalysts[37]. However, it is now quantified for the first time that these differences in activity would lead, in this specific case study, to a difference in light-off temperatures as high as 240 K in an adiabatic fixed-bed reactor.

The four catalysts differed not only in terms of T_{LO} but also in the shape of their light-off curves, which was compared in terms of tgα, i.e. the slope of the tangent to the curve at T_{LO}. This parameter can be considered as a measure for temperature control within an adiabatic fixed-bed reactor: the steeper the light-off curve, the more pronounced the effect of a small increase in the inlet temperature around T_{LO} will be on both the outlet oxygen conversion and, consequently, the peak temperature in the reactor.

Table 2 reports tgα, together with the selectivity to C_{2+} hydrocarbons achieved for $T_0 = T_0^*$ and the corresponding adiabatic temperature rise for each catalyst.

Table 2. Slope of the tangent to the light-off curve, selectivity to C_{2+} hydrocarbons and adiabatic temperature rise corresponding to $T_0=T_0^*$, for the four catalysts reported in Figure 5. Operating conditions: $CH_4/O_2|_{z=0}= 12$, $p_t= 150$ kPa, no gas-phase dilution, GHSV= 35000 h^{-1}, $W/F_{CH4,0}= 3.45\ kg_{cat}\ s/mol_{CH4,0}$.

Catalyst	**tgα (K^{-1})**	**S_{C2+} for $T_0=T_0^*$ (-)**	**Adiabatic Temperature Rise for $T_0= T_0^*$ (K)**
La-Sr/CaO	$16.6 \cdot 10^{-2}$	45%	411
Sr/La_2O_3	$16.4 \cdot 10^{-2}$	62%	394
Sn-Li/MgO	$3.9 \cdot 10^{-2}$	84%	343
$NaMnW/SiO_2$	$3.4 \cdot 10^{-2}$	90%	271

tgα was found to be a good indicator of the selectivity towards C_{2+} products at iso-oxygen conversion, with the least selective catalysts giving rise to steeper curves. This is due to the previously mentioned inverse relationship between selectivity and adiabatic temperature rise: the non-selective oxidation reactions to CO_x generate more thermal power than the coupling reaction, thus increasing reaction rates more rapidly and bringing the system to complete oxygen depletion. Therefore comparing the shapes of light-off curves of different OCM catalysts simulated at the same operating conditions can be used as a measure of the 'explosiveness' of the reaction.

The impact of the operating conditions on the light-off curves was evaluated for the $4\%_{wt}$Sn-$2\%_{wt}$Li/MgO catalyst: space time, pressure, methane to oxygen inlet ratio, gas-phase dilution and particle diameter were analyzed. The results are reported in the Supporting Information and are summarized as follows: every change in the operating conditions which results in an

increase in conversion and/or a decrease in C_{2+} selectivity, leads to a decrease in light-off temperature and an increase in tgα. Among the investigated variables, changes in the space time and inlet composition were found to be the most influential on the light-off temperature and, together with the inlet temperature, were selected as the main manipulation variables for the next section of the study. For a quantification of the above mentioned effects, the reader is referred to paragraph 6 of the Supporting Information.

3.3 Tuning the operating conditions for low temperature – high yield operation

Light-off curves have shown to be powerful tools in identifying and comparing the minimum inlet temperature required for the adiabatic operation of OCM catalytic beds. This was regarded as the first step in the selection of suitable OCM catalysts and it served as preliminary guideline in the performance-oriented analysis, which is going to be presented in this section.

The C_{2+} *ultimate* yield, obtained by adjusting the space time in order to simulate the performances of all catalysts at complete oxygen conversion at the reactor outlet, was herein considered as the main catalyst selection criterion.

An optimal yield was obtained each time by fine-tuning the operating conditions: more specifically the inlet temperature T_0 and the reactants molar inlet ratio $CH_4/O_2|_{z=0}$. The operating pressure was fixed to the value of 150 kPa to reduce the degrees of freedom. The choice of low pressure, already anticipated in section 3.1, was further sustained by the light-off study reported in the Supporting Information (Fig. S4).

Four additional operational constraints were imposed in the tuning procedure:

(i) $T_0 < 923$ K, this being the primary goal of a low inlet temperature adiabatic fixed-bed reactor for OCM;

(ii) $T^{max} \leq 1273$ K, as maximum work temperature for non-refractory lined stainless steel reactors[57];

(iii) GHSV $\geq 1000\ h^{-1}$, in order to limit the maximum reactor size;

(iv) C_{2+} selectivity $\geq$ 60%, to limit separation train duties downstream the OCM reactor.

Conditions (iii) and (iv) were based on the patents of Siluria Technologies[58, 59] as the lowest reported values for GHSV and C_{2+} selectivity; therefore, in the present work they were considered as the threshold for the economic viability of an adiabatic OCM process.

Figure 6 shows the investigated ranges for T_0 and $CH_4/O_2|_{z=0}$ for the $1\%_{wt}Sr/La_2O_3$ catalyst, reported as contour plots of the maximum temperature in the reactor T^{max} and the C_{2+} *ultimate* yield. In order to achieve complete oxygen conversion at the reactor outlet, the GHSV was varied in the range 1100-82000 h^{-1}, corresponding to a space time variation in the range of 1.57 – 116.63 $kg_{cat}/mol_{CH4,0}$.

The trend in T^{max} at a given reactants inlet ratio clearly follows the increasing T_0. For a fixed inlet temperature, T^{max} is linked to the adiabatic temperature rise, in turn depending on the C_{2+} selectivity: a low reactant inlet ratio promotes non-selective oxidation reactions, thus leading to more exothermicity. For this reason, increasing $CH_4/O_2|_{z=0}$ lower T^{max} were obtained even when operating the reactor under higher T_0.

The C_{2+} *ultimate* yield follows the same trend as the temperature: the maximum methane conversion that can be achieved at complete oxygen conversion increases with a decreasing inlet ratio, and both conversion and selectivity are improved at higher inlet temperatures.

With respect to the maximum temperature allowed, only the part framed by yellow line satisfies constraint (ii): the highest C_{2+} yields simulated were discarded as they were obtained at T^{max} exceeding 1273 K. The maximum yield that satisfied all four constraints amounts to only 8% (at T_0= 723K, $CH_4/O_2|_{z=0}$ = 8.7), which is in strong contrast with the 26% (at T_0= 850K, $CH_4/O_2|_{z=0}$ = 5) obtained at a T^{max} of 1521 K.

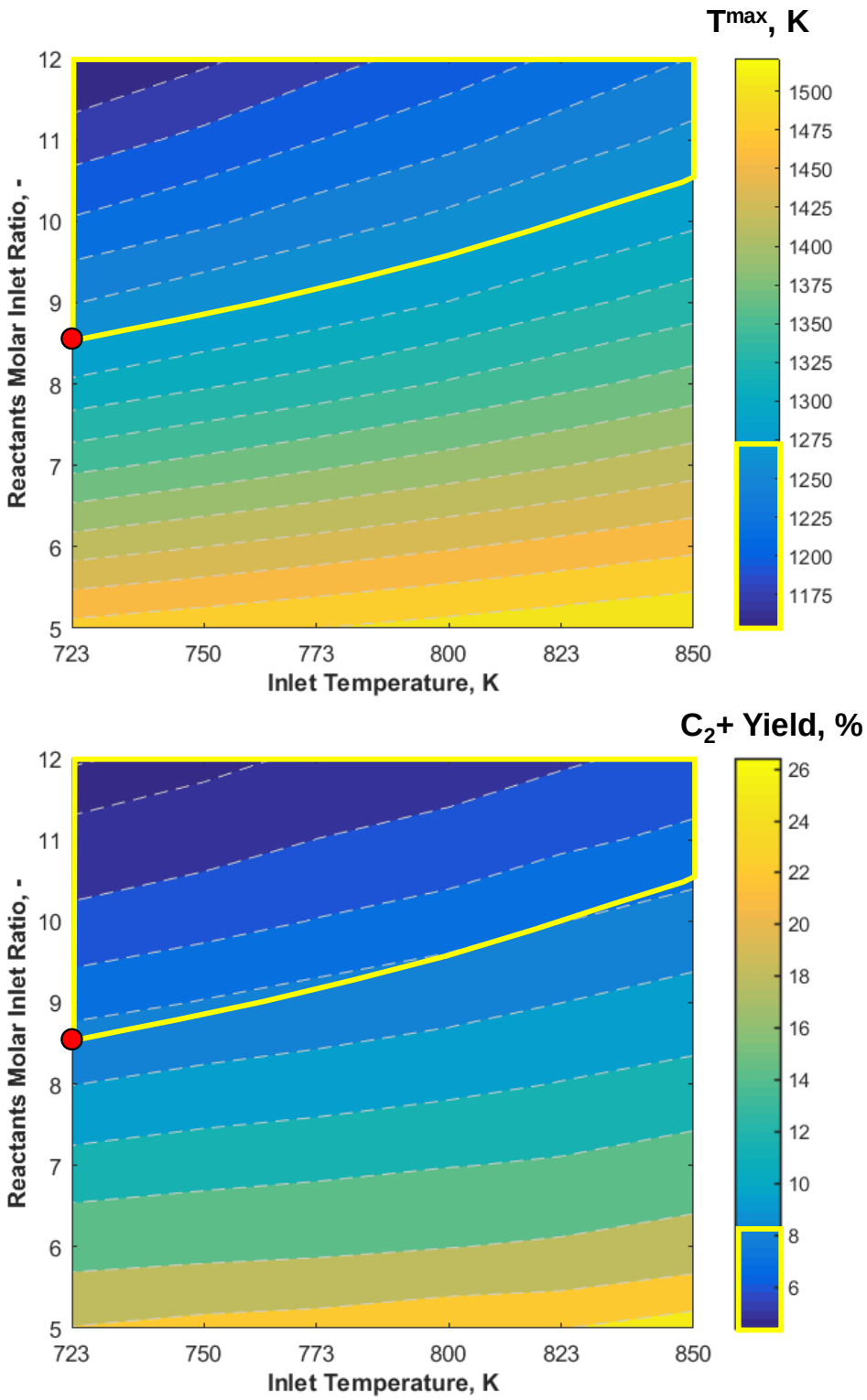

Figure 6. Contour plots of the maximum temperature in the adiabatic reactor T^{max} and the C_{2+} ultimate yield as a function of T_0 and $CH_4/O_2|_{z=0}$, for a 1%$_{wt}$Sr/La_2O_3 catalytic bed. Operating conditions: p_r= 150 kPa, complete oxygen conversion at the reactor outlet, GHSV =1100-82000 h^{-1}, $W/F_{CH4,0}$= 1.57 – 116.63 $kg_{cat}/mol_{CH4,0}$. The yellow lines identify the region of acceptable maximum temperature $T^{max} \leq$ 1273 K The red dot indicates the optimal operating point in this region.

By analyzing the yellow-framed part of the plane, the simulated C_{2+} *ultimate* yield slightly increases at lower inlet temperatures. This is due to the higher adiabatic temperature rise that is allowed when operating at lower T_0, which in turn allows a lower $CH_4/O_2|_{z=0}$. The resulting increase in methane conversion overcompensates the decrease in selectivity due to a more oxygen rich feed and leads to an overall increase in the yield.

The optimal operating point with respect to C_{2+} yield is indicated by the red dot in Figure 6: p_t= 150 kPa, T_0= 723 K, $CH_4/O_2|_{z=0}$ = 8.7, GHSV= 1110 h^{-1}, $W/F_{CH4,0}$= 111.40 kg_{cat} $s/mol_{CH4,0}$. The obtained performances were: X_{CH4}= 13%, S_{C2+}= 61%, Y_{C2+}= 8% and ΔT^{ad}= 550 K. Due to the low values of GHSV and $S_{C2+,}$ the inlet temperature was not further reduced.

By comparing these values with the results reported in Figure 2, it can be observed that the rational fine-tuning of the operating conditions led to a 33% increase in the simulated C_{2+} *ultimate* yield, without penalizing the selectivity and at the same time fulfilling the required operational constraints.

It is worth highlighting that, when increasing the inlet temperature along the yellow line in Figure 6 up to T_0= 850K, the decrease in Y_{C2+} (from 8% to 7%) is accompanied by a drastic decrease in the space time required to achieve complete oxygen conversion (from 111.40 kg_{cat} $s/mol_{CH4,0}$ to 2.66 kg_{cat} $s/mol_{CH4,0}$). One of the performance indicators which is mostly affected by this temperature-related difference in the catalyst activity is the Space Time Yield of C_{2+} products (C_{2+} STY), defined as the mol_{C2+} produced per unit of time per kg of catalyst. The STY in the two limiting operating points of the yellow line (T_0=723K, $CH_4/O_2|_{z=0}$= 8.7) and (T_0= 850K, $CH_4/O_2|_{z=0}$= 10.6) increases from $3.60 \cdot 10^{-4}$ to $1.35 \cdot 10^{-2}$ mol_{C2+} s/kg_{cat}). The advantage in terms of low inlet temperature operation and higher C_{2+} yield comes, hence, at the expense of the overall productivity. For this reason, also the C_{2+} STY is going to be considered in the comparison with the other catalytic materials.

The prior analysis of light-off curves (specifically, Figure S7 of the Supporting Information) suggested that the utilization of air as oxidant would mitigate the adiabatic temperature rise due to the presence of nitrogen as a diluent in the feed. In order to verify whether this could lead to an additional improvement in the *ultimate* yield, a similar fine-tuning of the operating conditions was performed using air as oxidizing agent, instead of pure oxygen. The contour plots for T^{max} and C_{2+} *ultimate* yield are reported in Figure 7. As expected, the maximum temperatures obtained were lower compared to the undiluted case and, as a result, a higher amount of oxygen (i.e. lower $CH_4/O_2|_{z=0}$) could be fed to the reactor. By assuming a simplified air composition of 79 mol% N_2 and 21 mol% O_2 and the range of investigated reactant inlet ratio ($CH_4/O_2|_{z=0}$= 5 - 10), the corresponding nitrogen dilution in the gas feed ranged from 38.5 to 25.5 mol%. The sum of the reactant partial pressures (CH_4 and O_2) always amounted to p_r= 150 kPa to make a correct comparison. As a result, the total pressure had to be adapted for each inlet ratio to compensate for the presence of N_2, ranging from 240 kPa bar for $CH_4/O_2|_{z=0}$= 5 to 200 kPa for $CH_4/O_2|_{z=0}$= 10.

Figure 7 suggests an alternative operating point for a Sr/La_2O_3 adiabatic catalytic bed in presence the of air instead of pure oxygen, indicated by the red dot in Figure 7: p_t= 220 kPa, T_0= 750 K, $CH_4/O_2|_{z=0}$ = 7.3, 31.1 mol% N_2, GHSV= 2260 h^{-1}, $W/F_{CH4,0}$= 55.80 kg_{cat} $s/mol_{CH4,0}$. The obtained performances were: X_{CH4}= 15%, S_{C2+}= 60%, Y_{C2+}= 9% and ΔT^{ad}= 523 K.

Comparing these figures with the pure oxygen case, a slight increase in maximum achievable C_{2+} *ultimate* yield was observed (from 8% to 9%). Indeed temperature mitigation by nitrogen allows a lower reactant molar inlet ratio ($CH_4/O_2|_{z=0}$= 7.3 vs 8.7), thus higher methane conversion (X_{CH4}= 15% vs 13%), while simultaneously maintaining T^{max} below the limiting value of 1273 K. However the T_0 required in the presence of air (T_0= 750 K) had to be higher compared to the case with pure oxygen (T_0= 723 K), following constraint (iv) on the C_{2+} selectivity owing to the higher relative amount of oxygen present in the feed.

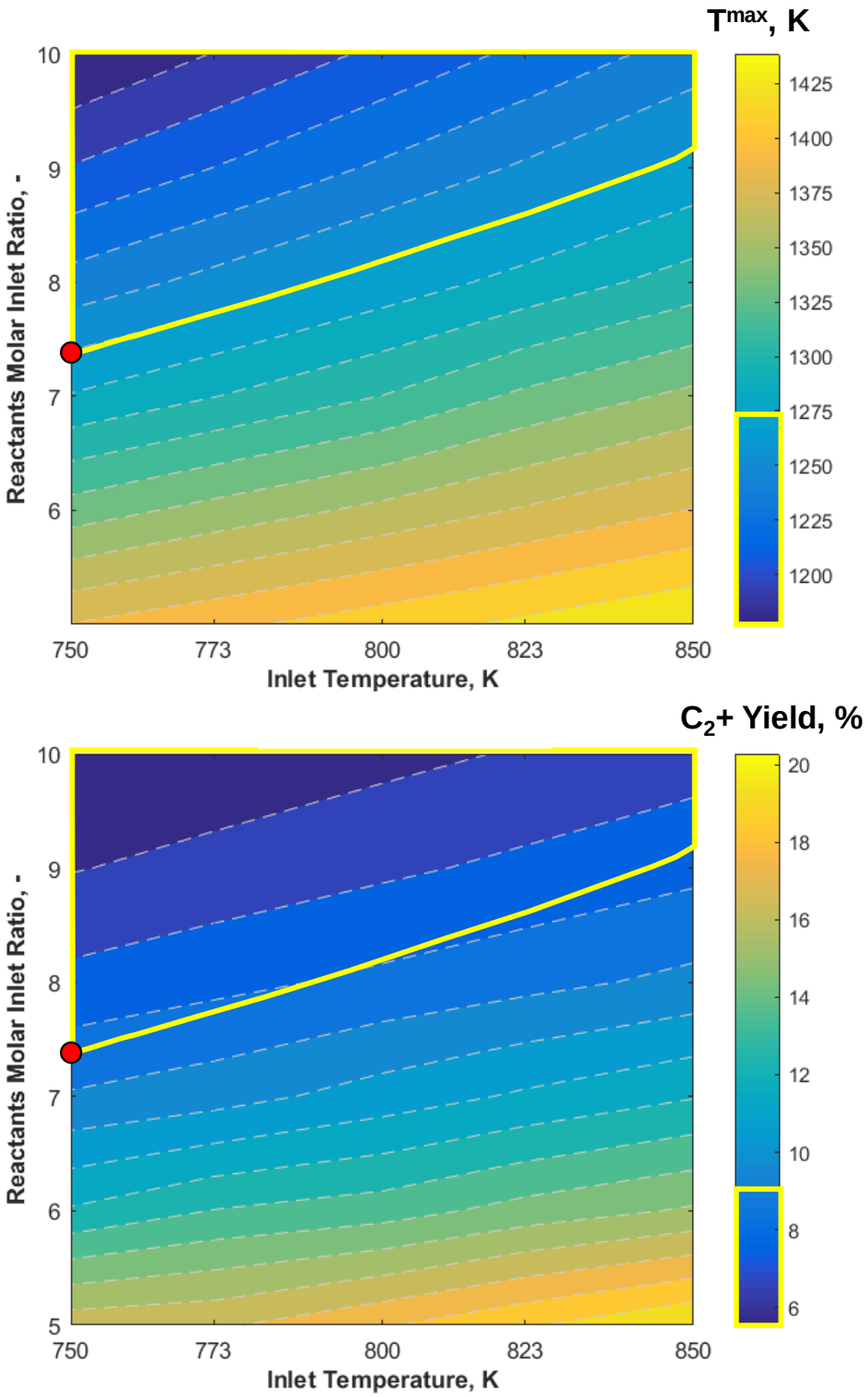

Figure 7. Contour plots of the maximum temperature in the adiabatic reactor T^{max} and the C_{2+} ultimate yield as a function of T_0 and $CH_4/O_2|_{z=0}$, for a 1%$_{wt}$Sr/La_2O_3 catalytic bed with air co-feeding, instead of pure oxygen. Operating conditions: p_r= 150 kPa, complete oxygen conversion at the reactor outlet, GHSV =2150-39200 h^{-1}, $W/F_{CH4,0}$= 3.11 – 13.52 $kg_{cat}/mol_{CH4,0}$. Nitrogen mol% in the feed varies from 38.5% (for $CH_4/O_2|_{z=0}$= 5) to 25.5% (for $CH_4/O_2|_{z=0}$= 10).The yellow lines identify the region of acceptable maximum temperature T^{max}≤ 1273 K. The red dot indicates the optimal operating point in this region.

An analogous procedure, considering only pure oxygen, was followed for the other three catalysts, using the prior analysis of light-off curves as a guideline for the identification of potential operating intervals. The optimal operating conditions for each of them are reported in Table 3 in order of increasing *ultimate* yield.

Table 3. Optimal operating conditions and corresponding adiabatic ultimate performances of the four catalysts in exam, assuming pure oxygen as oxidizing agent. The underlined value indicates that operational constraint (iv) was not met in the tuning procedure. The GHSV values reported in the table correspond to a space time variation in the range $W/F_{CH4,0}$ *= 0.97 – 125.70* kg_{cat} *s/*$mol_{CH4,0.}$

Catalyst	**T_0 (K)**	**$CH_4/O_2|_{z=0}$ (-)**	**GHSV (h^{-1})**	**ΔT^{ad} (K)**	**X_{CH4} (%)**	**S_{C2+} (%)**	**Y_{C2+} (%)**	**C_{2+} STY ($mol_{C2+}\ s^{-1}\ kg_{cat}^{-1}$)**
La-Sr/CaO	850	10.9	125600	423	9	**<u>53</u>**	5	$2.38 \cdot 10^{-2}$
Sr/La_2O_3	723	8.7	1100	550	13	61	8	$3.60 \cdot 10^{-4}$
Sn-Li/MgO	750	8.5	1040	523	18	79	14	$5.64 \cdot 10^{-4}$
$NaMnW/SiO_2$	853	8.9	1060	420	19	82	16	$6.62 \cdot 10^{-4}$

The CaO based catalyst, which, according to the comparison of light-off curves, seemed the most suitable for low temperature operation, did not meet the requirement of minimum desired selectivity (condition (iv)). Despite the very high activity, and the consequent high C_{2+} STY obtained, the maximum C_{2+} selectivity that could be achieved, while simultaneously fulfilling conditions (i), (ii) and (iii), was 53% and is indicated in bold and underlined in Table 3; this value was obtained via a high reactant molar inlet ratio, which in turn reduced the methane conversion and limited the overall yield to 5%. It could be concluded that the most active, but least selective catalyst, proved to be the least suitable for a profitable adiabatic operation.

The MgO based catalyst exhibits a more moderate activity compared to the La_2O_3 based one, as previously highlighted from the light-off curves analysis. Therefore T_0 had to be limited to 750 K due to the GHSV constraint (iii). However, its high selectivity, as seen from isothermal data[60], led to a promising C_{2+} yield of 14% in adiabatic operation. In terms of C_{2+} STY, the increase in selectivity resulted into a higher productivity compared to the La_2O_3 catalyst, even if the GHSV was comparable. Nevertheless, it has to be verified to what extent the Sn-Li/MgO

catalyst is stable at the high temperatures considered: concerns about its stability and thermal resistance were previously shown also for the isothermal operation[61].

The activity of the NaMnW/SiO_2 catalyst is rather low compared to the other investigated catalysts; this is in line with the experimental results[62] and had already emerged as a limiting factor during the evaluation of light-off curves. For this reason, for this catalyst a higher T_0 had to be selected (853 K) in order meet the other operational constraints. Thanks to the high selectivity of this catalyst, the C_{2+} yield amounted to 16% corresponding to the highest value obtained in the present work while respecting the maximum temperature constraint. Also in terms of C_{2+} STY the NaMnW/SiO_2 catalyst showed the highest productivity, among those fulfilling the minimum selectivity criterion. However also for this catalyst, high-temperature stability might be a challenge[22].

On the basis of these results, it was concluded that high activity is not sufficient to achieve a desired low inlet temperature operation of an OCM adiabatic fixed-bed. In contrast to what was a priori expected, less active but more selective catalysts seem to be more relevant, following the reduction in adiabatic temperature rise. The drawback in terms of activity could be compensated by a slight increase in inlet temperature or a higher amount of catalyst, even if the latter choice penalized the output in terms of productivity.

These results highlight that the search for an optimal OCM catalyst cannot be treated independently from the selected reactor configuration, given the limited extrapolability of isothermal results to adiabatic operation, and pave the way for a future optimization work both in terms of catalyst properties and operating conditions.

The performances reported in Table 3, which are in line with the experimental ones reported in a recent patent application from SABIC[63], are still far away from the threshold value of 30% yield, commonly adopted from the work of Kuo et al.[64], for OCM economic viability. However, due the modified economic context in comparison with 1989, in the recent literature[65] lower

yields are also considered acceptable for the industrial feasibility of the OCM reaction, as long as selectivity exceeds 80%. Therefore, the C_{2+} *ultimate* yields simulated in the present study for the most selective catalysts (Sn-Li/MgO and NaMnW/SiO_2) are to be considered encouraging for the scale-up of the process in its adiabatic configuration.

4. CONCLUSIONS

The present work highlighted the performances of well-known OCM catalysts, previously assessed at isothermal operating conditions, in adiabatic fixed-bed reactors. The relationship between C_{2+} selectivity and temperature, affecting both the adiabatic temperature rise in the reactor and the achievable C_{2+} yield, was addressed as the major additional challenge of adiabatic OCM.

The analysis of light-off curves aided in identifying operating temperature ranges for different catalysts, providing insights both in activity and C_{2+} selectivity in adiabatic operation.

These insights were used as starting point for the rational tuning of the operating conditions for each of the above catalysts, aimed at maximizing the C_{2+} *ultimate* yield maximization at preferably low inlet temperatures. The major constraint limiting the achievable yield at complete oxygen conversion was found to be the maximum allowable temperature in the reactor. With this constraint, the *ultimate* yield increased at lower inlet temperatures and catalyst selectivity rather than activity was identified as the key feature to boost yields.

The obtained results indicated that data from isothermal operation are not easily extrapolatable to adiabatic operation and that the search for an optimal OCM catalyst should always be tailored to the adopted reactor configuration.

The C_{2+} yields herein simulated for selective catalysts are considered promising enough to encourage the design of adiabatic experiments, to be complemented with catalyst stability tests

(up to 1273 K), aimed at identifying optimal catalyst-operating configuration combinations for an economically viable implementation of OCM.

Supporting Information

Gas phase and surface reaction networks; summary of catalyst descriptors used in the microkinetic model; elucidation on the reactor model equations and numerical procedure; description of particle-scale temperature gradients and relative equations; graphs reporting the influence of operating variables on the position and the shape of the light-off curves of the Sn-Li/MgO catalyst.

AUTHOR INFORMATION

Corresponding author

* Email: Joris.Thybaut@ugent.be

ACKNOWLEDGMENTS

This work was supported by the Research Program Agreement, with reference Total/IPA-4999 & UGent/A15-TT-1487, between TOTAL Research & Technology Feluy and Ghent University.

The authors would like to thank Dr. Jonas Van Belleghem and Dr. Pedro Mendes for the valuable insights provided, respectively, in the initial and final stage of the work. JWT acknowledges the ERC for the PoC grant SERENiTi (GA n° 825783).

NOTATION

Roman Letters

C_2	$C_2H_6 + C_2H_4 + C_2H_2$

C_{2+}		$C_2H_6 + C_2H_4 + C_2H_2 + C_3H_8 + C_3H_6$
$CH_4/O_2\|_{z=0}$		reactants molar inlet ratio
d_p	[m]	particle diameter
d_v	[m]	average distance between two catalyst pellets
F	[mol s^{-1}]	molar flow rate
GHSV	[h^{-1}]	Gas Hourly Space Velocity: ratio of the volumetric Flow rate of reactants ($CH_4 + O_2$) at standard conditions (Sm^3/h) and the vessel volume (m^3)
L	[m]	reactor length
p_r	[kPa]	partial pressure of the reactants
p_t	[kPa]	total pressure
r	[m]	particle-scale interstitial coordinate
S_i		selectivity of species i, $S_i = \frac{(F_i - F_{i,0})}{(F_{CH4,0} - F_{CH4})}$
STY	[mol s^{-1} kg_{cat}^{-1}]	Space Time Yield of a specified product
T	[K]	temperature
W	[kg]	catalyst mass
x	[m]	axial reactor coordinate
X_i		conversion of species i, $X_i = \frac{(F_{i,0} - F_i)}{F_{i,0}}$
Y_i		yield of species i, $Y_i = X_{CH4} \cdot S_i$
z		dimensionless axial reactor coordinate

Greek Letters

tgα	[K^{-1}]	slope of the tangent to the light-off curve at T_{LO}
ΔT^{ad}	[K]	adiabatic temperature rise
ξ	[m]	particle-scale intraparticle coordinate

Sub- and Superscripts

0	reactor inlet
c	catalyst particle
g	gas-phase
interst	interstitial
intrap	intraparticle
L	reactor outlet
LO	light-off

* complete oxygen conversion at reactor outlet

REFERENCES

(1) Keller, G. E.; Bhasin, M. M. Synthesis of Ethylene via Oxidative Coupling of Methane. I. Determination of Active Catalysts. *J. Catal.* **1982,** *73*, 9-19.

(2) Schwach, P.; Pan, X. L.; Bao, X. H. Direct Conversion of Methane to Value-Added Chemicals over Heterogeneous Catalysts: Challenges and Prospects. *Chem. Rev.* **2017,** *117*, 8497-8520.

(3) Kee, R. J.; Karakaya, C.; Zhu, H. Y. Process Intensification in the Catalytic Conversion of Natural Gas to Fuels and Chemicals. *Proc. Combust. Inst.* **2017,** *36*, 51-76.

(4) Stangland, E. E. Shale Gas Implications for C_2-C_3 Olefin Production: Incumbent and Future Technology. *Annu. Rev. Chem. Biomol. Eng.* **2018,** *9*, 341-364.

(5) Friedel, M.; Nitzsche, J.; Krause, H. Catalyst Screening and Reactor Modeling for Oxidative Methane Coupling to Increase the Heating Value of Biogas. *Chem. Ing. Tech.* **2017,** *89*, (6), 715-723.

(6) Amghizar, I.; Vandewalle, L. A.; Van Geem, K. M.; Marin, G. B. New Trends in Olefin Production. *Engineering* **2017,** *3*, (2), 171-178.

(7) Ren, T.; Patel, M. K.; Blok, K. Steam Cracking and Methane To Olefins: Energy Use, CO_2 Emissions and Production Costs. *Energy* **2008,** *33*, 817-833.

(8) Sinev, M. Y. Modeling of Oxidative Transformations of Light Alkanes over Heterogeneous Catalysts. *Russ. J. Phys. Chem. B* **2007,** *1*, 412-433.

(9) Su, Y. S.; Ying, J. Y.; Green, W. H. Upper Bound on the Yield for Oxidative Coupling of Methane. *J. Catal.* **2003,** *218*, 321-333.

(10) Korf, S. J.; Roos, J. A.; Ross, J. R. H. The Development of Doped Li/MgO Catalyst Systems for the Low-Temperature Oxidative Coupling of Methane. In *Methane Conversion by Oxidative Processes: Fundamental and Engineering Aspects*, Wolf, E. E., Ed. Van Nostrand Reinhold: 1992; pp 168-199.

(11) Pak, S.; Lunsford, J. H. Thermal Effects during the Oxidative Coupling of Methane over $Mn/Na_2WO_4/SiO_2$ and Mn/Na_2WO_4/MgO Catalysts. *Appl. Catal. A-Gen.* **1998,** *168*, 131-137.

(12) Gambo, Y.; Jalil, A. A.; Triwahyono, S.; Abdulrasheed, A. A. Recent Advances and Future Prospect in Catalysts for Oxidative Coupling of Methane to Ethylene: a Review. *J. Ind. Eng. Chem.* **2018,** *59*, 218-229.

(13) Cruellas, A.; Melchiori, T.; Gallucci, F.; van Sint Annaland, M. Advanced Reactor Concepts for Oxidative Coupling of Methane. *Catal. Rev.-Sci. Eng.* **2017,** *59*, 234-294.

(14) Salerno, D.; Godini, H. R.; Penteado, A.; Esche, E.; Wozny, G. Techno-Economic Evaluation of an Oxidative Coupling of Methane Process at Industrial Scale Production. In *26th European Symposium on Computer Aided Process Engineering*, Kravanja, Z.; Bogataj, M., Eds. Elsevier Science Bv: Amsterdam, 2016; Vol. 38B, pp 1785-1790.

(15) Spallina, V.; Velarde, I. C.; Jimenez, J. A. M.; Godini, H. R.; Gallucci, F.; van Sint Annaland, M. Techno-Economic Assessment of Different Routes for Olefins Production through the Oxidative Coupling of Methane (OCM): Advances in Benchmark Technologies. *Energy Convers. Manage.* **2017,** *154*, 244-261.

(16) Annapragada, A. V.; Gulari, E. Fe-P-O Catalysts for Methane Utilization Catalyst Development and Identification. *J. Catal.* **1990,** *123*, 130-146.

(17) Aseem, A.; Jeba, G. G.; Conato, M. T.; Rimer, J. D.; Harold, M. P. Oxidative Coupling of Methane over Mixed Metal Oxide Catalysts: Steady State Multiplicity and Catalyst Durability. *Chem. Eng. J.* **2018,** *331*, 132-143.

(18) Lee, J. Y.; Jeon, W.; Choi, J. W.; Suh, Y. W.; Ha, J. M.; Suh, D. J.; Park, Y. K. Scaled-up Production of C_2 Hydrocarbons by the Oxidative Coupling of Methane over Pelletized $Na_2WO_4/Mn/SiO_2$ Catalysts: Observing Hot Spots for the Selective Process. *Fuel* **2013,** *106*, 851-857.

(19) Noon, D.; Seubsai, A.; Senkan, S. Oxidative Coupling of Methane by Nanofiber Catalysts. *ChemCatChem* **2013,** *5*, 146-149.

(20) Noon, D.; Zohour, B.; Senkan, S. Oxidative Coupling of Methane with La_2O_3-CeO_2 Nanofiber Fabrics: a Reaction Engineering Study. *J. Nat. Gas Sci. Eng.* **2014,** *18*, 406-411.

(21) Tarasov, A. L.; Kustov, L. M. Autothermal Methane Oxidative Coupling Process over La_2O_3/MgO Catalysts. *Chem. Eng. Technol.* **2015,** *38*, 2243-2252.

(22) Sarsani, S.; West, D.; Liang, W. G.; Balakotaiah, V. Autothermal Oxidative Coupling of Methane with Ambient Feed Temperature. *Chem. Eng. J.* **2017,** *328*, 484-496.

(23) Degnan, T. Siluria and OCM – Close to Full Scale Commercializaton? *Focus on Catalysts* **2016,** *2016*, 1-2.

(24) Iyer, R.; Tkachenko, A.; Weinberger, S.; Scher, E. C.; Zurcher, F. R.; Cizeron, J. M.; Schammel, W. P.; Gamoras, J.; Karshtedt, D.; Nyce, G. Natural Gas Processing and Systems. U.S. Patent 9,670,113 B2, 2017.

(25) Gemini - Oxidative Coupling of Methane (OCM). https://www.linde-engineering.com/en/process_plants/petrochemical-plants/oxidative-coupling-methane/index.html (Accessed 08/10/2018).

(26) Karakaya, C.; Zhu, H.; Loebick, C.; Weissman, J. G.; Kee, R. J. A Detailed Reaction Mechanism for Oxidative Coupling of Methane over $Mn/Na_2WO_4/SiO_2$ Catalyst for Non-Isothermal Conditions. *Catal. Today* **2018,** *312*, 10-22.

(27) Sun, Z.; West, D. H.; Balakotaiah, V. Bifurcation Analysis of Catalytic Partial Oxidations in Laboratory-Scale Packed-Bed Reactors with Heat Exchange. *Chem. Eng. J.* **2018**.

(28) Balakotaiah, V.; West, D. H. Thermal Effects and Bifurcations in Gas Phase Catalytic Partial Oxidations. *Curr. Opin. Chem. Eng.* **2014,** *5*, 68-77.

(29) Sinev, M. Y.; Fattakhova, Z. T.; Lomonosov, V. I.; Gordienko, Y. A. Kinetics of Oxidative Coupling of Methane: Bridging the Gap Between Comprehension and Description. *J. Nat. Gas Chem.* **2009,** *18*, 273-287.

(30) Duprat, F. Light-off Curve of Catalytic Reaction and Kinetics. *Chem. Eng. Sci.* **2002,** *57*, 901-911.

(31) Santamaria, J. M.; Miro, E. E.; Wolf, E. E. Reactor Simulation Studies of Methane Oxidative Coupling on a Na/$NiTiO_3$ Catalyst. *Ind. Eng. Chem. Res.* **1991,** *30*, 1157-1165.

(32) Tye, C. T.; Mohamed, A. R.; Bhatia, S. Modeling of Catalytic Reactor for Oxidative Coupling of Methane using La_2O_3/CaO Catalyst. *Chem. Eng. J.* **2002,** *87*, 49-59.

(33) Hoebink, J. H. B. J.; Couwenberg, P. M.; Marin, G. B. Fixed Bed Reactor Design for Gas Phase Chain Reactions Catalysed by Solids: the Oxidative Coupling of Methane. *Chem. Eng. Sci.* **1994,** *49*, 5453-5463.

(34) Stansch, Z.; Mleczko, L.; Baerns, M. Comprehensive Kinetics of Oxidative Coupling of Methane over the La_2O_3/CaO Catalyst. *Ind. Eng. Chem. Res.* **1997,** *36*, 2568-2579.

(35) Kechagiopoulos, P. N.; Thybaut, J. W.; Marin, G. B. Oxidative Coupling of Methane: a Microkinetic Model Accounting for Intraparticle Surface-Intermediates Concentration Profiles. *Ind. Eng. Chem. Res.* **2014,** *53*, 1825-1840.

(36) Alexiadis, V. I.; Thybaut, J. W.; Kechagiopoulos, P. N.; Chaar, M.; Van Veen, A. C.; Muhler, M.; Marin, G. B. Oxidative Coupling of Methane: Catalytic Behaviour Assessment via Comprehensive Microkinetic Modelling. *Appl. Catal. B-Environ.* **2014,** *150*, 496-505.

(37) Alexiadis, V. I.; Chaar, M.; van Veen, A.; Muhler, M.; Thybaut, J. W.; Marin, G. B. Quantitative Screening of an Extended Oxidative Coupling of Methane Catalyst Library. *Appl. Catal. B-Environ.* **2016,** *199*, 252-259.

(38) Sun, Z.; Kota, A.; Sarsani, S.; West, D. H.; Balakotaiah, V. Bifurcation Analysis of Methane Oxidative Coupling Without Catalyst. *Chem. Eng. J.* **2018,** *343*, 770-788.

(39) Vandewalle, L. A.; Lengyel, I.; West, D. H.; Van Geem, K. M.; Marin, G. B. Catalyst Ignition and Extinction: a Microkinetics-Based Bifurcation Study of Adiabatic Reactors for Oxidative Coupling of Methane. *Chem. Eng. Sci.* **2018**.

(40) Karakaya, C.; Zhu, H. Y.; Zohour, B.; Senkan, S.; Kee, R. J. Detailed Reaction Mechanisms for the Oxidative Coupling of Methane over La_2O_3/CeO_2 Nanofiber Fabric Catalysts. *ChemCatChem* **2017,** *9*, (24), 4538-4551.

(41) Carberry, J. J.; Wendel, M. M. A Computer Model of the Fixed Bed Catalytic Reactor: the Adiabatic and Quasi-Adiabatic Cases. *AiChE J.* **1963,** *9*, 129-133.

(42) Mears, D. E. Diagnostic Criteria for Heat Transport Limitations in Fixed Bed Reactors. *J. Catal.* **1971,** *20*, 127-131.

(43) Wijngaarden, R. J.; Westerterp, K. R. The Role of Pellet Thermal-Stability in Reactor Design for Heterogeneously Catalyzed Chemical-Reactions. *Chem. Eng. Sci.* **1992,** *47*, 1517-1522.

(44) Please, C. P.; Hagan, P. S.; Schwendeman, D. W. Light-off Behavior of Catalytic-Converters. *SIAM J. Appl. Math.* **1994,** *54*, 72-92.

(45) Lang, W.; Laing, P.; Cheng, Y.; Hubbard, C.; Harold, M. P. Co-oxidation of CO and Propylene on Pd/CeO_2-ZrO_2 and Pd/Al_2O_3 Monolith Catalysts: a Light-off, Kinetics and Mechanistic Study. *Appl. Catal. B-Environ.* **2017,** *218*, 430-442.

(46) Ramanathan, K.; Balakotaiah, V.; West, D. H. Light-off Criterion and Transient Analysis of Catalytic Monoliths. *Chem. Eng. Sci.* **2003,** *58*, 1381-1405.

(47) Wang, Y. Q.; Xiao, L.; Zhao, C. C.; Liu, F.; Li, S. Catalytic Combustion of Toluene with $Pd/La_{0.8}Ce_{0.2}MnO_3$ Supported on Different Zeolites. *Environ. Prog. Sustain. Energy* **2018,** *37*, 215-220.

(48) Fan, Z. Y.; Fang, W. J.; Zhang, Z. X.; Chen, M. X.; Shangguan, W. F. Highly Active Rod-like Co_3O_4 Catalyst for the Formaldehyde Oxidation Reaction. *Catal. Commun.* **2018,** *103*, 10-14.

(49) Hinokuma, S.; Shimanoe, H.; Kawabata, Y.; Matsuki, S.; Kiritoshi, S.; Machida, M. Effects of Support Materials and Silver Loading on Catalytic Ammonia Combustion Properties. *Catal. Today* **2018,** *303*, 2-7.

(50) Lee, J. H.; Trimm, D. L. Catalytic Combustion of Methane. *Fuel Process. Technol.* **1995,** *42*, 339-359.

(51) Bharadwaj, S. S.; Schmidt, L. D. Catalytic Partial Oxidation of Natural Gas to Syngas. *Fuel Process. Technol.* **1995,** *42*, (2), 109-127.

(52) Gartner, C. A.; van Veen, A. C.; Lercher, J. A. Oxidative Dehydrogenation of Ethane: Common Principles and Mechanistic Aspects. *ChemCatChem* **2013,** *5*, (11), 3196-3217.

(53) Mleczko, L.; Baerns, M. Catalytic Oxidative Coupling of Methane - Reaction-Engineering Aspects and Process Schemes. *Fuel Process. Technol.* **1995,** *42*, 217-248.

(54) Gu, T.; Balakotaiah, V. Analysis of Upstream Creeping Reaction Zones in Catalytic Monolith Reactors. *Chem. Eng. J.* **2017,** *317*, 267-279.

(55) Choudhary, V. R.; Rane, V. H. Acidity Basicity of Rare-Earth-Oxides and their Catalytic Activity in Oxidative Coupling of Methane to C_2 Hydrocarbons. *J. Catal.* **1991,** *130*, (2), 411-422.

(56) Albrecht, M.; Rodemerck, U.; Linke, D.; Kondratenko, E. V. Oxidative Coupling of Methane at Elevated Pressures: Reactor Concept and its Validation. *React. Chem. Eng.* **2018,** *3*, 151-154.

(57) Crook, P. Corrosion Resistant Nickel Alloys - Part 2. *Adv. Mater. Process.* **2007,** *165*, (7), 31-33.

(58) Duggal, S. R., G.; Mccormick, J.; Aronson, A.; Cizeron, J.; Jonnavittula, D. Separation Methods and Systems for Oxidative Coupling of Methane. U.S. Patent Application Publication 2014/0012053 A1, 2017.

(59) Cizeron, J.; Radaelli, G.; Lakhapatri, S.; Freer, E.; Hong, J. K.; McCormik, J.; Sheridan, D.; Reid, C.; Pellizzari, R.; Weinberger, S.; Edwards, J. D. Reactors and Systems for Oxidative Coupling of Methane. U.S. Patent 10,047,020 B2, 2018.

(60) Korf, S. J.; Roos, J. A.; Veltman, L. J.; van Ommen, J. G.; Ross, J. R. H. Effect of Additives on Lithium Doped Magnesium-Oxide Catalysts used in the Oxidative Coupling of Methane. *Appl. Catal.* **1989,** *56*, 119-135.

(61) Arndt, S.; Laugel, G.; Levchenko, S.; Horn, R.; Baerns, M.; Scheffler, M.; Schlogl, R.; Schomacker, R. A Critical Assessment of Li/MgO-Based Catalysts for the Oxidative Coupling of Methane. *Catal. Rev.-Sci. Eng.* **2011,** *53*, (4), 424-514.

(62) Malekzadeh, A.; Abedini, M.; Khodadadi, A. A.; Amini, M.; Mishra, H. K.; Dalai, A. K. Critical Influence of Mn on Low-Temperature Catalytic Activity of $Mn/Na_2WO_4/SiO_2$ Catalyst for Oxidative Coupling of Methane. *Catal. Lett.* **2002,** *84*, 45-51.

(63) Liang, W.; Sarsani, S.; West, D.; Lowrey, J.; Mamedov, A.; Lengyel, I. Low Inlet Temperature for Oxidative Coupling of Methane. U.S. Patent Application Publication 2018/0162785 A1, 2018.

(64) Kuo, J. C. W.; Kresge, C. T.; Palermo, R. E. Evaluation of Direct Methane Conversion to Higher Hydrocarbons and Oxygenates. *Catal. Today* **1989,** *4*, 463-470.

(65) Kondratenko, E. V.; Peppel, T.; Seeburg, D.; Kondratenko, V. A.; Kalevaru, N.; Martin, A.; Wohlrab, S. Methane Conversion into Different Hydrocarbons or Oxygenates: Current Status and Future Perspectives in Catalyst Development and Reactor Operation. *Catal. Sci. Technol.* **2017,** *7*, 366-381.

FOR TABLE OF CONTENTS ONLY